Filling the gap: A 60 ky record of mixed carbonate-siliciclastic turbidite deposition from the Great Barrier Reef

Ángel Puga-Bernabéu, Jody M. Webster, Robin J. Beaman, Paula J. Reime, Willem Renema

Marine and Petroleum Geology 50 (2014) 40–50

Contents lists available at ScienceDirect

Marine and Petroleum Geology

journal homepage: www.elsevier.com/locate/marpetgeo

Filling the gap: A 60 ky record of mixed carbonate-siliciclastic turbidite deposition from the Great Barrier Reef

Ángel Puga-Bernabéu [a,b,*], Jody M. Webster [b], Robin J. Beaman [c], Paula J. Reimer [d], Willem Renema [e]

[a] Departamento de Estratigrafía y Paleontología, Universidad de Granada, 18002 Granada, Spain
[b] Geocoastal Group, School of Geosciences, The University of Sydney, NSW 2006, Australia
[c] School of Earth and Environmental Sciences, James Cook University, PO Box 6811, Cairns, QLD 4870, Australia
[d] School of Geography, Archaeology and Palaeoecology, Queen's University Belfast, Belfast, BT7 1NN Northern Ireland, UK
[e] Naturalis Biodiversity Center, PO Box 9517, 2300 RA Leiden, The Netherlands

ARTICLE INFO

Article history:
Received 1 July 2013
Received in revised form
3 November 2013
Accepted 12 November 2013
Available online 20 November 2013

Keywords:
Turbidites
Submarine canyons
Slope morphology
Shelf-edge barrier reef
Sequence stratigraphy
North-eastern Australia margin

ABSTRACT

Late Pleistocene to Holocene margin sedimentation on the Great Barrier Reef, a mixed carbonate-siliciclastic margin, has been explained by a transgressive shedding model. This model has challenged widely accepted sequence stratigraphic models in terms of the timing and type of sediment (i.e. carbonate vs. siliciclastic) deposited during sea-level oscillations. However, this model documents only hemipelagic sedimentation and the contribution of coarse-grained turbidite deposition, and the role of submarine canyons in this process, remain elusive on this archetypal margin. Here we present a new model of turbidite deposition for the last 60 ky in the north-eastern Australia margin. Using high-resolution bathymetry, 58 new and existing radiometric ages, and the composition of 81 turbidites from 15 piston cores, we found that the spatial and temporal variation of turbidites is controlled by the relationship between sea-level change and the variable physiography along the margin. Siliciclastic and mixed carbonate-siliciclastic turbidites were linked to canyons indenting the shelf-break and the well-developed shelf-edge reef barriers that stored sediment behind them. Turbidite deposition was sustained while the sea-level position allowed the connection and sediment bypassing through the inter-reef passages and canyons. Carbonate turbidites dominated in regions with more open conditions at the outer-shelf and where slope-confined canyons dominated or where canyons are generally less abundant. The turn-on and maintenance of carbonate production during sea-level fluctuations also influenced the timing of carbonate turbidite deposition. We show that a fundamental understanding of the variable physiography inherent to mixed carbonate-siliciclastic margins is essential to accurately interpret deep-water, coarse-grained deposition within a sequence stratigraphic context.

1. Introduction

In the last decade, the generic reciprocal and highstand shedding models of margin sedimentation (Wilson, 1967; Droxler and Schalger, 1985; Posamentier and Vail, 1988) were challenged by the transgressive shedding or coeval model (Page et al., 2003; Francis et al., 2007) established in the Great Barrier Reef, the largest extant mixed carbonate-siliciclastic system found on the north-eastern Australia margin. This alternative model, based on the study of hemipelagic sediments from the slope and basin (Dunbar et al., 2000; Page et al., 2003), argues that maximum siliciclastic fluxes to the slope since the Last Glacial Maximum occurred during the late transgression ca. 11–7 ka, rather than when sea level was at lowstand before 18 ka as the generic models predict. Further, the accumulation of siliciclastic and carbonate sediments varies coevally, although the accumulation of carbonates during the sea-level highstand is higher than of siliciclastics (Page et al., 2003).

However, the coeval model is focused exclusively on hemipelagic sedimentation and is thus decoupled from turbidite deposition. Therefore, the model likely overlooks the significant contribution of turbidite deposition to the sediment accumulation on slope and basin settings, as commonly occurs in either carbonate margins (Bornhold and Pilkey, 1971; Crevello and Schalger, 1980) or siliciclastic margins (Covault and Romans, 2009; Ducassou et al., 2009).

* Corresponding author. Departamento de Estratigrafía y Paleontología, Universidad de Granada, 18002 Granada, Spain. Tel.: +34 958 242721; fax: +34 958 248528.
E-mail address: angelpb@ugr.es (Á. Puga-Bernabéu).

0264-8172/$ – see front matter © 2013 Elsevier Ltd. All rights reserved.
http://dx.doi.org/10.1016/j.marpetgeo.2013.11.009

Further, in other mixed carbonate-siliciclastic systems, such as the Gulf of Papua, turbidite deposition is not fully consistent with a coeval model (Jorry et al., 2008, 2010). Recently, Webster et al. (2012) found that canyon turbidite sedimentation in the north-eastern Australia margin is locally different to the existing models of margin sedimentation, highlighting the important role of canyons and shelf morphology in this process. Therefore, a better knowledge of the regional turbidite deposition and timing is needed in order to postulate a comprehensive sedimentation model for mixed carbonate-siliciclastic margins.

In this study, we present a turbidite deposition model for the north-eastern Australia margin based on 38 new and 20 existing radiometric ages and sedimentologic data from sediment cores, together with the accurate geomorphic context of the collected cores provided by high-resolution multibeam bathymetry data. We interpret this model as a result of the interaction of the Late Pleistocene sea-level fluctuations together with the variable margin physiography.

2. Regional setting

We focused our investigation in three study areas characterized by different shelf and slope morphologies within the north-eastern Australia margin between latitudes 14°30′S and 18°30′S: Ribbon Reef, Noggin Passage and Palm Passage (Fig. 1A). The Ribbon Reef region comprises a narrow (<50 km) flat shelf, rimmed by an extensive shelf-edge reef barrier system (the Ribbon Reefs), with a shelf-break at ~70 m. The steep (>6°) continental slope is deeply excavated by shelf-incised canyons (Fig. 1A, B), named the Ribbon Reef Canyons (Puga-Bernabéu et al., 2011). The connection of the Ribbon Reef Canyons with the shelf is influenced by the Ribbon Reefs and the inter-reef passages between them, which are locally connected to shelf-paleochannels (Webster et al., 2012). In contrast, the broader (60–65 km) gently sloping shelf in the Noggin Passage region exhibits more open conditions at the outer-shelf due to the lack of near-continuous reef barriers. The shelf-break at ~102–109 m (Abbey et al., 2011) connects with a moderately (~4°) steep slope with sigmoidal depth profiles. The slope is shaped by the Noggin Canyons, which mostly comprise slope-confined canyons (Fig. 1A, C; Puga-Bernabéu et al., 2013). In the Palm Passage region, the shelf widens up to 125 km with discontinuous submerged terraces and the shelf-break at ~102–103 m (Abbey et al., 2011). The gently (<2°) dipping slope is wider (up to 40 km) than in Ribbon Reef and Noggin Passage regions (Fig. 1A). This region of the slope is not incised by well-developed canyons, and the few that exist mostly comprise slope-confined canyons especially in the southern part where the slope is narrower (Fig. 1A). However, the slope in the Palm Passage region is shaped by abundant landslides, with widths ranging from a few kilometers to about 20 km (Fig. 1D).

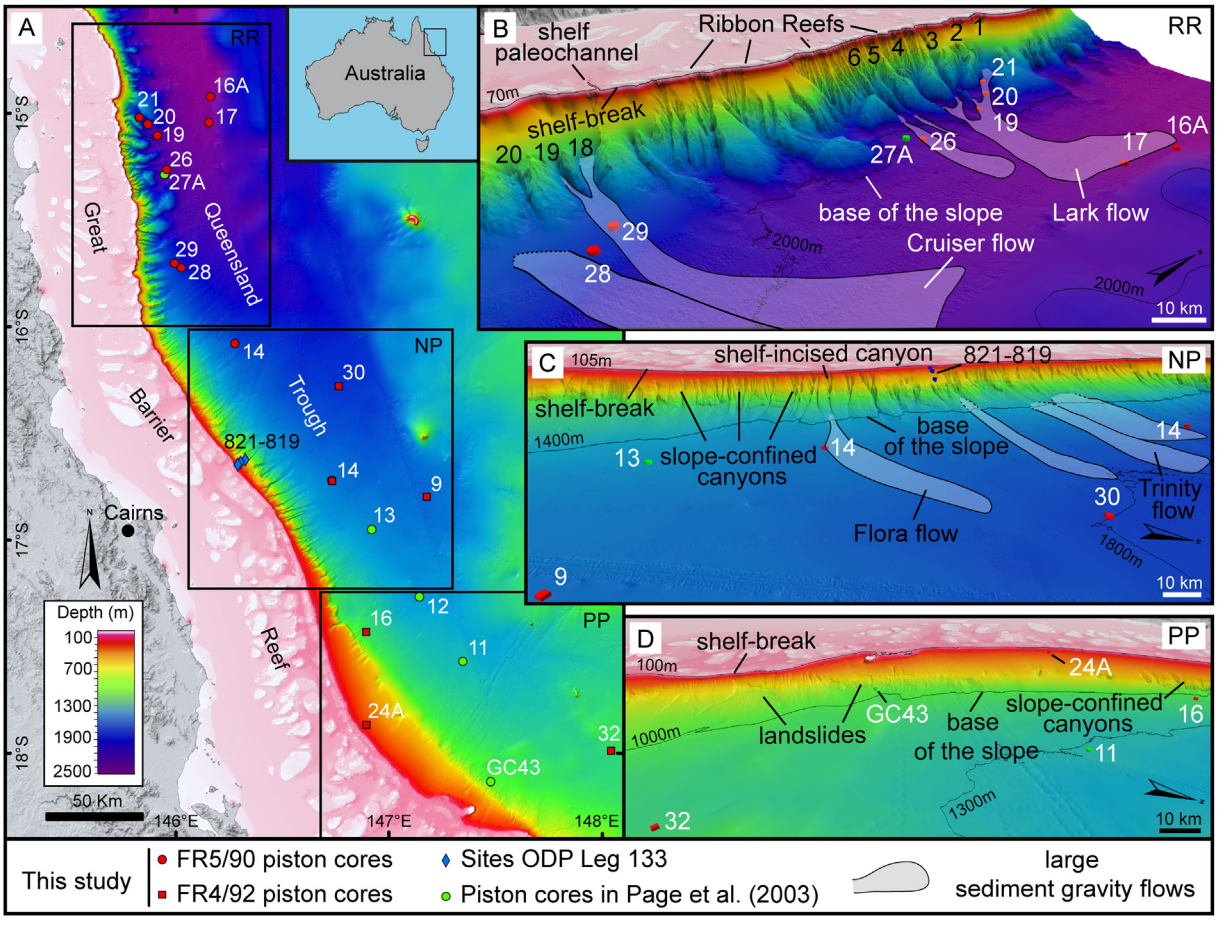

Figure 1. (A) Bathymetry (100 m-resolution DEM) of the north-eastern Australia margin showing the location of the study areas and cores (insets): Ribbon Reef = RR, Noggin Passage = NP, Palm Passage = PP. (B), (C) and (D) illustrate DEMs of the study areas (color scale as in (A); vertical exaggeration is 6). Location of large sediment gravity flows is shown (based on sidescan sonar data from HMAS *Cook* in 1989; names after Dunbar et al., 2000). The location of piston cores studied by Page et al. (2003) used to establish the transgressive shedding model, are also labeled for context. Similarly, the long cores from the Ocean Drilling Program (ODP Leg 133) are also shown. Note the different shelf morphology, canyon types and seabed features along the margin providing detailed the geomorphic context of the different cores. (For interpretation of the references to color in this figure legend, the reader is referred to the web version of this article.)

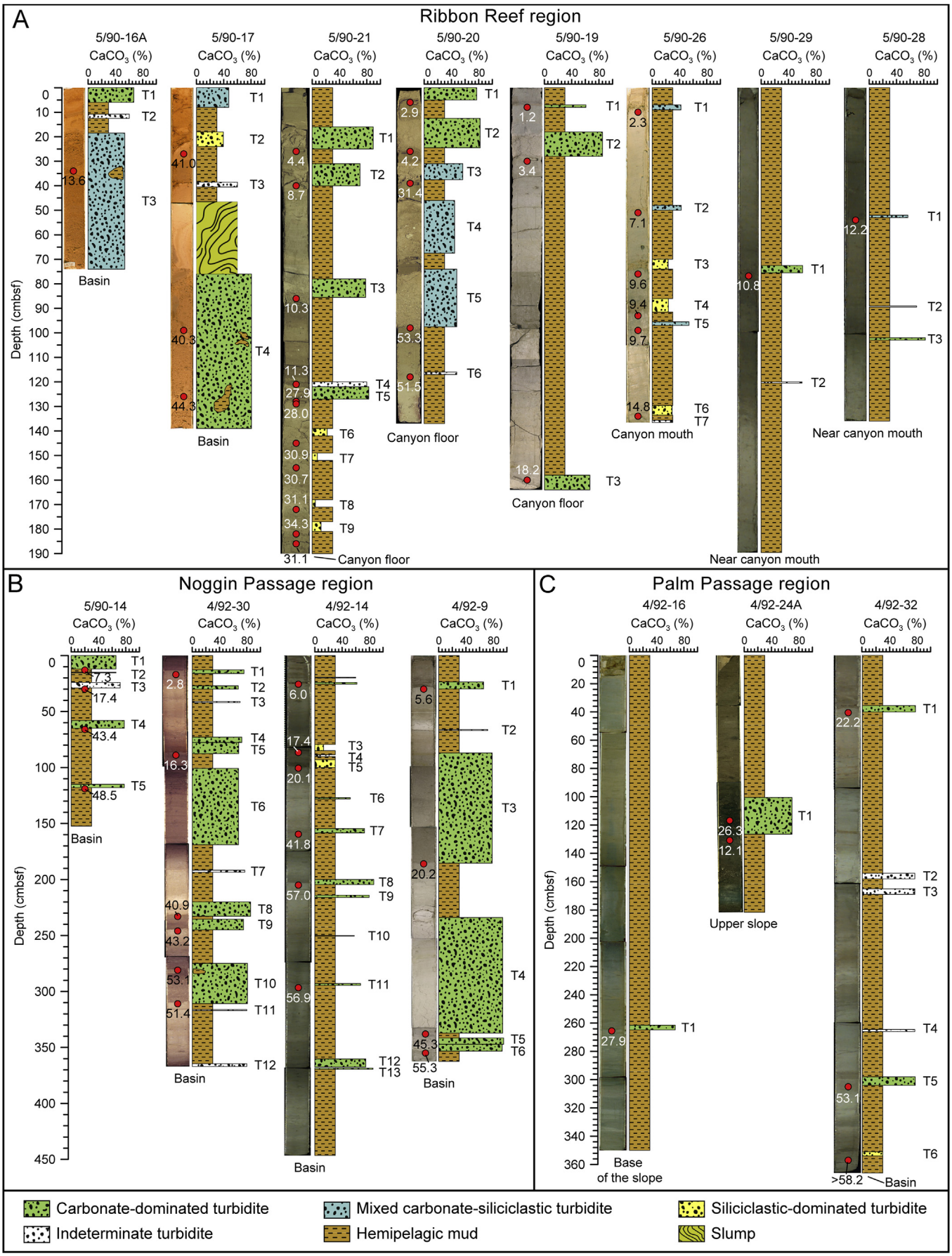
A
Ribbon Reef region
5/90-16A
5/90-17
5/90-21
5/90-20
5/90-19
5/90-26
5/90-29
5/90-28
CaCO3 (%)
0 40 80
Depth (cmbsf)
Basin
Canyon floor
Canyon mouth
Near canyon mouth
B
Noggin Passage region
5/90-14
4/92-30
4/92-14
4/92-9
C
Palm Passage region
4/92-16
4/92-24A
4/92-32
Upper slope
Base of the slope
>58.2
Carbonate-dominated turbidite
Mixed carbonate-siliciclastic turbidite
Siliciclastic-dominated turbidite
Indeterminate turbidite
Hemipelagic mud
Slump

3. Material and methods

Available bathymetry data (100 m-resolution grid) for the entire margin (Beaman, 2010) were enhanced by two close-up views of the Ribbon Reef (40 m-resolution grid) and Noggin Passage (30 m-resolution grid) regions. High-resolution multibeam data were collected using a Simrad EM300 multibeam echosounder (30 kHz) during the RV *Southern Surveyor* cruise in 2007 and 2008 (Tilbrook and Matear, 2008; Webster et al., 2008). Fifteen piston cores collected on RV *Franklin Cruises* (FR5-90 and FR4/92), herein named 90/core or 92/core, were examined in this study (Figs. 1 and 2). The sixty two piston cores collected below 200 m depth during these expeditions represent the most complete dataset of slope and basin subsurface sediments in the north-eastern Australia margin until present-day. However, most of these cores were collected far from canyon sources and not all of them contain sediment gravity flow deposits (Dunbar et al., 2000). Additional subsurface sediment data come from long cores of the Ocean Drilling Program Leg 133 (Fig. 1; Davies et al., 1991).

In addition to the three cores studied by Webster et al. (2012) in the Ribbon Reef region, we selected twelve cores with sandy deposits interbedded with hemipelagic muds. Here, we use the generic term turbidite to refer to these sand- to gravel-size sediments. The distinction of the accurate type of sediment gravity flow (e.g. debrites, high-density turbidites, low-density turbidites, mudflows, etc.) and other aspects as flow transformation during deposition are not considered in this study.

In contrast to previous studies based on low-resolution bathymetry, we can place the study cores within an accurate geomorphic context in relation to their canyon sources (Fig. 1, Tables 1 and 2). In the Ribbon Reef region (Fig. 1A, B), 90/19 to 21 are located on the floor of Canyon 1 (Webster et al., 2012), 90/26 was collected close to the mouth of Canyon 6, 90/29 is located at the mouth of Canyons 18 and 19, and 90/28 is sourced from Canyon 20. Further, 90/16 and 17, located over the Lark flow (after Dunbar et al., 2000) in the deepest part of the Queensland Trough, were presumably sourced from Canyons 1 to 6 (Fig. 1B). In the Noggin Passage region, the four selected cores (90/14, 92/09, 92/14 and 92/30) are located on the basin floor, close to the Trinity and Flora flows (after Dunbar et al., 2000). In the Palm Passage region, selected cores were collected on the upper slope (92/24A), the base of the slope (92/16) and in the basin (92/32).

Turbidite deposits were classified following Webster et al. (2012) as siliciclastic-dominated (<40% $CaCO_3$), carbonate-dominated (>60% $CaCO_3$), and mixed carbonate-siliciclastic (40–60% $CaCO_3$). The proportion of $CaCO_3$% was estimated by measuring the total carbon content of the samples (0.25–2 g) using an Elementar VarioMAX CNS analyzer and a LECO CNS TruSpec analyzer. These samples were collected in the lower part of the turbidites. The overall composition of thin turbidites (<1 cm) were estimated using visual identification on the cores and their relationship with over- and underlying turbidites. Turbidite deposits whose composition could not be determined were classified as indeterminate turbidites.

38 new ages were provided by mass spectrometry (AMS) radiocarbon analyses of individual planktonic foraminifera sampled from the hemipelagic muds directly underlying each turbidite deposit, and in a few cases, where the base the turbidites was not recovered, also from hemipelagic mudclasts within the turbidites (Fig. 2; Table 1). Bulk hemipelagic mud, 2 cm-thick samples were wet sieved at 125 μm, then washed and dried in an oven at 40 °C. After inspecting their preservation and rejecting specimens with any secondary cement, chamber infilling or discoloration, >300 individual planktonic foraminifera, mainly mixed layer (<100 m) species (e.g. *Globigerinoides ruber*, *Globigerinoides trilobus* and *Globigerinoides conglobatus*) were selected for each AMS-C14 measurement.

Turbidite chronologies can be determined using three main approaches, but all of them are subject to some uncertainty in establishing the true age of turbidite emplacement (see Owen et al., 2007 for a review). Dating the sediment or material within the turbidites provides the age the material deposited, but not the timing of the turbidite emplacement. Dating pelagic sediment immediately above the turbidites provides the age of the youngest sediment and therefore it might represent the ideal situation. However, it is not always possible to differentiate between the overlaying muds and the topmost part of the turbidites or because bioturbation is concentrated in this boundary, which can produce mixed ages on top of the turbidite. The third option is to date the pelagic sediment immediately below the turbidites, which provides the maximum age of the turbidite emplacement. However, in some circumstances this last method can produce biased ages, towards older ages, if significant portions of the pelagic material were eroded by the turbidite base. On the balance of the inherent inaccuracies in all the dating methods, for our study turbidite chronology follows the third option, i.e. dating the hemipelagic sediment underlying the turbidites. This provides an accurate maximum age of turbidite deposition without the ambiguity of distinguishing between the top of the turbidite (the "tail") and the overlying muds and the effect of bioturbation (Goldfinger et al., 2007). Although turbidite flows, are by their nature turbulent flows and cause erosion of the seafloor, most of the study cores are in a distal position, far from the canyon axis (Fig. 1) where erosion is generally higher (Beaubouef et al., 1999; Baztan et al., 2005). In one case (sample 92/24A_24) the age record comes from shell remains emplaced within the turbidite bed (Table 1).

All radiocarbon ages <48 ^{14}C yrs BP were converted to calibrated ages BP (ka) using CALIB 6.1.1 (Marine09.14C "global" marine calibration dataset described in Reimer et al., 2009) with ages reported with 2σ errors. This calibration takes into account a correction for the average ocean reservoir (*R*) (400 yrs) as well as a mean local deviation (Δ*R*) for north-eastern Australia of 12 ± 13 ^{14}C yrs. (Druffel and Griffin, 1993, 1999; Ulm, 2002). After first correcting for similar average ocean reservoir (*R*) (400 yrs) affects, the two ages >48 ^{14}C ka were converted to approximate calibrated BP ages (ka) using CalPal-2007 (Weninger et al., 2007). However, given the very old ages and small sample sizes, these measurements more conservatively represent "background" ages of at least older than about 50 ka.

4. Results

4.1. Turbidite types

Carbonate content analyses indicate that turbidite deposition is essentially carbonate-dominated along the north-eastern Australia margin (Fig. 2; Table 3). Carbonate turbidites comprise ~62% of the studied turbidites. These turbidites include fragments of shallow-water bioclasts (e.g. corals, coralline algae, mollusks, larger benthic foraminifera) as well as deep-water planktonic and small

Figure 2. Study cores in (A) Ribbon Reef region, (B) Noggin Passage region, and (C) Palm Passage region. The core data shows core logs, $CaCO_3$%, turbidite number (T) and C14-AMS age (calibrated BP ka). Carbonate content only provided for turbidites. Hemipelagic muds are represented with a fixed width for illustration purposes. The image of archive core 5/90-14 is not available. The depositional context of each core is also given (see Fig. 1 for detailed locations).

benthic foraminifera and pteropods (Webster et al., 2012), which locally constitute the bulk of the turbidites. In the siliciclastic-dominated turbidites, quartz grains are distinctive components (Webster et al., 2012). Mixed carbonate-siliciclastic and siliciclastic-dominated turbidites represent 12–15% of the turbidite deposition. However, the proportion of the different turbidite types is variable along the margin. In the Ribbon Reef region, the proportion of mixed carbonate-siliciclastic and siliciclastic turbidites is higher (~27%) than the average along the margin. These turbidites occur especially in cores related to shelf-incised canyons with heads close to the shelf-paleochannels (e.g. Canyons 1, 6, 18 and 19; Fig. 1A, B; Puga-Bernabéu et al., 2011; Webster et al., 2012). In the Noggin Passage region, turbidite deposition is fundamentally carbonate-dominated (~83%) and mixed carbonate-siliciclastic turbidites are absent. Only two siliciclastic turbidites occur in 92/14 (Fig. 2B). The location of 92/14 close to the Flora flow suggests that the turbidite deposits in this core are related to one of the few shelf-incised canyons in the Noggin Passage region (Fig. 1C). Turbidite deposition in the Palm Passage region is relatively scarce (eight events) and is mainly carbonate-dominated (Fig. 2C).

4.2. Timing and accumulation of turbidites

The 38 new and 20 existing calibrated radiocarbon ages range from >58.2 to 1.2 ka (Fig. 2; Table 1). The oldest ages (>50 ka) likely represent "background" ages. In the Ribbon Reef region, turbidite deposition >30 ka (MIS3) is characterized by siliciclastic and mixed carbonate-siliciclastic turbidites (Figs. 2A and 3A). These turbidites are associated with large shelf-incised canyons (e.g. Canyon 1, 90/19 to 21; Webster et al., 2012) and likely represent the continuation of high siliciclastic turbidite flows into the Queensland Trough (e.g. 90/17; Figs. 2A and 3A). Two carbonate turbidites were deposited between 30 and 15 ka (Fig. 3A) and were presumably sourced from the shelf-edge reefs (Webster et al., 2012). The interval between 15 and 7 ka records abundant and variable turbidite deposition (Fig. 3A). The youngest turbidites (<5 ka) are carbonate-dominated with only a single mixed carbonate-siliciclastic event at 2.3 ka (90/26; Figs. 2A and 3A). Cores in the Noggin Passage region record older carbonate turbidite deposition with several turbidites between 45 and 40 ka, and older events within the "background" age (Figs. 2B and 3B). Between 20 and 15 ka, both carbonate or siliciclastic turbidites were deposited on the seafloor of the Noggin Passage region, although the latter type only occurs in 92/14 (Fig. 2B). In contrast to the Ribbon Reef region, turbidite deposition in the Noggin Passage region is almost absent between 11 and 7 ka, with only one carbonate event recorded (Fig. 3B). Turbidite deposition <6 ka in the Noggin Passage region is carbonate-dominated, similar to the Ribbon Reef region. In the Palm Passage region, turbidite deposition is scarce and includes old (>50 ka), thin carbonate and siliciclastic turbidites (Figs. 2C and 3C). Two carbonate events occurred at ~28 and 22 ka at the base of the slope and in the basin (92/16 and 92/24; Figs. 2C and 3C). The youngest turbidite (~12 ka) in the upper slope of the Palm Passage region includes bioclastic reworked material (coral and bivalve fragments) of ~26 ka (Fig. 2C). Finally, there is a wide range in the thickness of turbidites emplaced at similar times in the three study regions (e.g. core 4/92-14-T5 and 4/92-9-T3 deposited at about 20 ka are respectively 3 cm and 98.4 cm thick; Fig. 2B; Table 1).

5. Discussion

Turbidite composition in the study region reflects the main sediment sources (i.e. terrigenous siliciclastics and biogenic carbonates) similar to the studies on hemipelagic sediments (Dunbar et al., 2000; Francis et al., 2007). However, our study demonstrates that the spatial accumulation and timing of the turbidites types differ along the margin (Fig. 3). Within the context of eustatic sea-level variability, we highlight the importance of the morphology of the shelf-edge and canyons in controlling turbidite deposition along the north-eastern Australia margin (Table 4).

The Ribbon Reef region shows the highest variability in the type and timing of turbidites deposited over the last 60 ky (Fig. 3A). We confirm that turbidite deposition during the transgression was not only carbonate-dominated (Webster et al., 2012) as a consequence of the initial shelf reflooding. The transgressive shedding model predicts that the highest hemipelagic siliciclastic fluxes occurred during the late transgression (11–7 ka; Dunbar and Dickens, 2003). We found that during this period (10–7 ka), siliciclastic and mixed carbonate-siliciclastic turbidite deposition also occurred as sea level was high enough (~15–30 m below present sea level) to completely flood the shelf and remobilize the sediment stored behind the shelf-edge reefs that had blocked supply to the slopes (e.g. Dunbar et al., 2000; Page et al., 2003). However, these sediments were likely funneled through the inter-reef passages and canyons and deposited into the basin (Fig. 1A, B), and not on the slope as previously suggested (Dunbar and Dickens, 2003; Page et al., 2003). Further, deposition of turbidites with high siliciclastic content started earlier than predicted in the transgressive shedding model, namely during late MIS2 when sea level was still below the depth of the local shelf-break (Fig. 3A). Those siliciclastic and mixed carbonate-siliciclastic turbidites deposited between 15 and 7 ka were funneled through canyons deeply incised into the shelf-break and connecting with the shelf-paleochannels existing between the Ribbon Reefs (e.g. Canyons 6 and 20; Figs. 1A and 3A). This process is largely controlled by the reef-blocking effect (Fig. 3A; Puga-Bernabéu et al., 2011) and the canyon type, and importantly, takes place mainly during sea-level heights that intersect and cross the inter-reef passages (e.g. Late MIS2 and MIS3; Webster et al., 2012). During the late Holocene (<6 ka), turbidite deposition is consistent with the highstand shedding model (i.e. carbonate-dominated; Droxler and Schalger, 1985). Episodic mixed carbonate-siliciclastic turbidite deposition during this period (90/26; Figs. 2 and 3) is also consistent with the local Holocene siliciclastic deposition suggested by Francis et al. (2007).

In the Noggin Passage region, the record of turbidite deposition over the last 60 ka is dominated by carbonate deposits independent of the sea-level position (Fig. 3B). In contrast to the Ribbon Reef region, the shelf-edge in the Noggin Passage region was not repeatedly intersected by MIS3 sea-level fluctuations as it lies deeper (~105 m). However, the deeper shelf-break allowed a greater depth window available for carbonate production on the outer-shelf during the MIS3 sea-level oscillations, likely related to the occurrence of fossil submerged reefs found in the area (Webster et al., 2011). Two other significant factors contribute to the different turbidite depositional patterns between the Noggin Passage and Ribbon Reef regions. First, the Noggin Canyons are mostly slope-confined, with the canyon heads deeper and further away from any siliciclastic sediments possibly stored on the shelf. Therefore, sediment funneled through these canyons was preferentially sourced from carbonate sediment produced in nearby submerged reefs and/or sediments from the upper slope and canyon settings. Second, the more open reef conditions at the outer-shelf, with a lack of well-developed reef barriers, favored the redistribution of sediment along the outer-shelf and dispersal to the upper slope. This physiography, together with the gently dipping outer-shelf and a deeper shelf-break allowed an earlier flooding of the shelf compared to the Ribbon Reef region. As a result, unconsolidated fine-grained hemipelagic sediments accumulated on the shelf during the sea-level lowstands could then be transported and deposited into deep-water settings (Dunbar et al.,

Table 1
Carbonate content, age data and methodology of study cores.

Core number[a]	Longitude (°E)	Latitude (°S)	Depth (m)	Depositional context	Turbidite event	Depth (cmbsf)	$CaCO_3$ content (%)	Turbidite type[b]	Sample number	Lab ID[c]	Sample depth (cmbsf)	Sample context	Radiocarbon ages (^{14}C yrs BP)	^{14}C yrs BP error	Calibrated ages BP (ka)	2σ age range (ka)
Ribbon Reef																
FR5/90 PC16A	146.163333	14.923333	2490	Basin (close to large SGF[d])	T1	0–6	67.2	C	N.A.[e]	N.A.	N.A.	N.A.	N.D.[f]	N.D.	N.D.	N.D.
					T2	10.8–12.5	N.D.	I	N.A.	N.A.	N.A.	N.A.	N.D.	N.D.	N.D.	N.D.
					T3	18.5–74	53.8	M	90/16A_67	UBA-11472	34	Hemipelagic mud clast within T3	12,170	36	13.60	13.44–13.75
FR5/90 PC17	146.155000	15.045000	2369	Basin (over large SGF)	T1	0–8	47.3	M	N.A.	N.A.	N.A.	N.A.	N.D.	N.D.	N.D.	N.D.
					T2	18–24	39.5	S	90/17_71	UBA-11473	27	Hemipelagic mud clast 3 cm below T2	36,279	316	41.01	40.35–41.67
					T3	38.5–40.5	N.D.	I	N.A.	N.A.	N.A.	N.A.	N.A.	N.A.	N.A.	N.A.
					T4	76–139	80.6	C	90/17_73	UBA-11474	99	Hemipelagic mud clast within T4	35,663	299	40.30	39.42–41.18
									90/17_75	UBA-11475	126	Hemipelagic mud clast within T4	40,873	342	44.32	43.66–44.97
									90/17_75	UBA-11475	126	Hemipelagic mud clast within T4	40,873	342	44.32	43.66–44.97
FR5/90 PC19	145.913333	15.106667	2220	Floor of Canyon 1 (canyon connected with shelf paleochannel)	T1	7–8	60.9	C	90/19_18	UBA-10556	8	Hemipelagic mud below T1	1637	25	1.19	1.11–1.27
					T2	18–28	85.1	C	90/19_3	OZJ835	30	Hemipelagic mud below T2	3580	50	3.46	3.3–3.59
					T3	158–163	66.7	C	90/19_6	OZJ836	160	Hemipelagic mud above T3	15,310	160	18.17	17.71–18.56
FR5/90 PC20	145.870000	15.051667	2110	Floor of Canyon 1 (canyon connected with shelf paleochannel)	T1	0–5	77.1	C	90/20_2	OZJ837	6	Hemipelagic mud below T1	3130	70	2.90	2.74–3.10
					T2	12.5–24.5	82.2	C	90/20_5	OZJ838	25.5	Hemipelagic mud below T2	2945	40	2.72	2.59–2.82
									90/20_5A	UBA-10555	26	Hemipelagic mud below T2	4164	25	4.22	4.12–4.35
					T3	31–37.5	56.6	M	90/20_8	OZJ839	39	Hemipelagic mud below T3	27,580	280	31.40	31.07–31.90
					T4	46–67.5	44.8	M	N.A.	N.A.	N.A.	N.A.	N.D.	N.D.	N.D.	N.D.
					T5	74–97.5	47.9	M	90/20_12	OZL169	98	Hemipelagic mud below T5	49,300	1500	53.34	50.57–56.11
					T6	116–117	N.D.	M?	90/20_19	OZL171	118	Hemipelagic mud below T6	48,000	1300	51.47	49.06–53.87
FR5/90 PC21	145.830000	15.021667	1982	Floor of Canyon 1 (canyon connected with shelf paleochannel)	T1	16–25	89.5	C	90/21_1	OZJ840	26	Hemipelagic mud below T1	4280	50	4.38	4.22–4.52
					T2	31–40	70.2	C	90/21_4	OZJ841	40	Hemipelagic mud below T2	8170	160	8.68	8.32–9.09
					T3	78–85.5	78.4	C	90/21_7	OZJ842	86	Hemipelagic mud below T3	9480	100	10.33	10.14–10.54
					T4	120–122	N.D.	C?	90/21_17	OZL174	121	Hemipelagic mud within T4	10,310	70	11.30	11.16–11.45
					T5	122–127	83.1	C	90/21_9	OZJ843	128	Hemipelagic mud below T5	23,460	230	27.86	27.42–28.46
									90/21_21	OZL175	129	Hemipelagic mud below T5	23,600	140	28.04	27.68–28.49
					T6	139–142	22.1	S	90/21_13	OZL170	145	Hemipelagic mud below T6	26,680	180	30.95	30.58–31.20
					T7	149–152	7.6	S	90/21_14	UBA-10554	155	Hemipelagic mud below T7	26,358	84	30.73	30.44–31.01

(*continued on next page*)

Table 1 (*continued*)

Core number[a]	Longitude (°E)	Latitude (°S)	Depth (m)	Depositional context	Turbidite event	Depth (cmbsf)	$CaCO_3$ content (%)	Turbidite type[b]	Sample number	Lab ID[c]	Sample depth (cmbsf)	Sample context	Radiocarbon ages (^{14}C yrs BP)	^{14}C yrs BP error	Calibrated ages BP (ka)	2σ age range (ka)
					T8	168–171	4.6	S	90/21_15	OZL172	172	Hemipelagic mud below T8	26,950	180	31.11	30.86–31.32
					T9	177–181	13.0	S	90/21_16	OZL173	182	Hemipelagic mud below T9	30,060	240	34.30	33.54–34.79
									90/21_22	OZL176	186	Hemipelagic mud 5 cm below T9	27,020	250	31.13	30.77–31.42
FR5/90 PC26	145.960000	15.266667	2210	Mouth of Canyon 6 (canyon connected to shelf paleochannel)	T1	7–9	42.1	M	90/26_8	UBA-15716	10	Hemipelagic mud below T1	2616	26	2.26	2.17–2.35
					T2	48–50	42.5	M	90/26_45	UBA-15717	51	Hemipelagic mud below T2	6562	33	7.06	6.95–7.16
					T3	70–74	23.4	S	90/26_67	UBA-15718	76	Hemipelagic mud below T3	8928	42	9.58	9.48–9.69
					T4	86–91.5	23.7	S	90/26_84	UBA-15719	93	Hemipelagic mud below T4	8777	42	9.45	9.37–9.53
					T5	95.5–97	53.9	M	90/26_91	UBA-15720	99	Hemipelagic mud below T5	8995	39	9.67	9.53–9.81
					T6	129.6–133.6	29.3	S	90/26_51	UBA-11469	134	Hemipelagic mud below T6	12,663	60	14.78	14.75–14.82
					T7	135.6–136.6	N.D.	I	N.A.	N.A.	N.A.	N.A.	N.D.	N.D.	N.D.	N.D.
FR5/90 PC28	146.026667	15.726667	1850	Near mouth of Canyons 19 and 20	T1	52–53	56.8	M	90/28_65	UBA-11471	54	Hemipelagic mud below T1	10,778	35	12.19	12.03–12.35
					T2	89–89.5	N.D.	I	N.A.	N.A.	N.A.	N.A.	N.D.	N.D.	N.D.	N.D.
					T3	102–103	82.3	C								
FR5/90 PC29	145.993333	15.705000	1834	Near mouth of Canyons 18 and 19	T1	72.5–75.5	60.8	C	90/29_61	UBA-10572	77	Hemipelagic mud below T1	9897	35	10.82	10.63–11.02
					T2	120–120.5	N.D.	I	N.A.	N.A.	N.A.	N.A.	N.D.	N.D.	N.D.	N.D.
Noggin Passage																
FR5/90 PC14	146.278333	16.080000	1724	Basin. close to large SGF	T1	0–12	65.6	C	90/14_16	UBA-15711	13	Hemipelagic mud below T1	6828	34	7.34	7.26–7.41
					T2	15–15.5	N.D.	C?	N.A.	N.A.	N.A.	N.A.	N.D.	N.D.	N.D.	N.D.
					T3	24–29	N.D.	C?	90/14_34	UBA-15712	30	Hemipelagic mud below T3	14,396	64	17.36	17.31–17.40
					T4	58–65	77.9	C	90/14_68	UBA-15713	66	Hemipelagic mud below T4	39,591	345	43.40	42.41–44.39
					T5	115–118	77.8	C	90/14_119	UBA-15714	119	Hemipelagic mud below T5	45,668	575	48.45	46.94–49.95
FR4/92 PC9	147.176333	16.795667	1616	Basin (closest canyons are slope-confined)	T1	23.6–29.8	66.0	C	92/09_29	UBA-15701	30	Hemipelagic mud below T1	5247	30	5.60	5.52–5.69
					T2	66–66.9	N.D.	C	N.A.	N.A.	N.A.	N.A.	N.D.	N.D.	N.D.	N.D.
					T3	87–185.4	78.4	C	92/09_186	UBA-15702	186	Hemipelagic mud below T3	17,543	63	20.18	19.93–20.43
					T4	234–337.2	93.9	C	92/09_336	UBA-15703	338	Hemipelagic mud below T4	42,286	414	45.28	44.61–45.96
					T5	341.5–347.1	95.2	C	N.A.	N.A.	N.A.	N.A.	N.D.	N.D.	N.D.	N.D.
					T6	347.1–353.3	93.1	C	92/09_355	UBA-15704	355	Hemipelagic mud below T5	51,090	981	55.28	52.99–57.57
FR4/92 PC14	146.732333	16.722833	1574	Basin (over large SGF connected to shelf-incised canyon)	T1	19.4–20	N.D.	I	92/14_5	UBA-10559	25.60	Hemipelagic mud below T1	5580	29	5.97	5.88–6.06
					T2	24–25.5	61.7	C	N.A.	N.A.	N.A.	N.A.	N.D.	N.D.	N.D.	N.D.
					T3	79.5–85	12.8	S	92/14_11	UBA-11466	86.60	Hemipelagic mud below T3	14,428	48	17.35	17.29–17.41
					T4	88.5–90.2	N.D.	S?	N.A.	N.A.	N.A.	N.A.	N.D.	N.D.	N.D.	N.D.
					T5	93–100	30.0	S	92/14_7	UBA-10560	100.60	Hemipelagic mud below T5	17,316	48	20.09	19.84–20.34

					T6	127–128	N.D.	C?	N.A.	N.A.	N.A.	N.A.	N.D.	N.D.	N.D.	N.D.
					T7	154.6–158.5	72.9	C	92/14_9	UBA-11465	159.60	Hemipelagic mud below T7	37,299	277	41.79	41.32–42.25
					T8	200–204.5	86.6	C	92/14_13	UBA-11467	205.00	Hemipelagic mud below T8	53,920	1726	57.00	54.84–59.16
					T9	214–216	79.7	C	N.A.	N.A.	N.A.	N.A.	N.D.	N.D.	N.D.	N.D.
					T10	250–250.5	N.D.	C?	N.A.	N.A.	N.A.	N.A.	N.D.	N.D.	N.D.	N.D.
					T11	293–294.5	67.2	C	92/14_21	UBA-10562	296.60	Hemipelagic mud below T11	52,983	904	56.85	54.76–58.94
					T12	360.3–367.5	74.8	C	N.A.	N.A.	N.A.	N.A.	N.D.	N.D.	N.D.	N.D.
					T13	368.5–369.5	85.4	C	N.A.	N.A.	N.A.	N.A.	N.D.	N.D.	N.D.	N.D.
FR4/92 PC30	146.763833	16.278330	1797	Basin	T1	12.7–16	75.9	C	92/30_27	UBA-10564	17	Hemipelagic mud below T1	2979	28	2.75	2.69–2.82
					T2	27–30	67.6	C	N.A.	N.A.	N.A.	N.A.	N.D.	N.D.	N.D.	N.D.
					T3	41–42	N.D.	C?	N.A.	N.A.	N.A.	N.A.	N.D.	N.D.	N.D.	N.D.
					T4	72.9–77.6	72.7	C	N.A.	N.A.	N.A.	N.A.	N.D.	N.D.	N.D.	N.D.
					T5	77.6–87.6	68.2	C	92/30_25	UBA-10563	89	Hemipelagic mud below T5	13,708	45	16.30	15.84–16.77
					T6	100.8–169	67.9	C	N.A.	N.A.	N.A.	N.A.	N.D.	N.D.	N.D.	N.D.
					T7	191.7–193.5	N.D.	C?	N.A.	N.A.	N.A.	N.A.	N.D.	N.D.	N.D.	N.D.
					T8	220–232.8	85.6	C	92/30_233	UBA-15707	233	Hemipelagic mud below T8	36,132	247	40.90	40.33–41.48
					T9	235.4–245	75.2	C	92/30_245	UBA-15708	246	Hemipelagic mud below T9	39,334	283	43.19	42.61–43.76
					T10	274.9–310.8	81.0	C	92/30_29	UBA-10565	281	Hemipelagic mud clast within T10	49,218	763	53.10	1970
									92/30_31	UBA-10566	311	Hemipelagic mud below T10	47,814	574	51.42	1630
					T11	316.1–317.1	N.D.	I	N.A.	N.A.	N.A.	N.A.	N.D.	N.D.	N.D.	N.D.
					T12	364.5–367	N.D.	I	N.A.	N.A.	N.A.	N.A.	N.D.	N.D.	N.D.	N.D.
Palm Passage																
FR4/92 PC16	146.892167	17.430833	1043	Base of the slope (close to large landslide scars and slope-confined canyon)	T1	261.5–264.8	67.3	C	92/16_262	UBA-15705	265.5	Hemipelagic mud below T1	23,421	95	27.88	27.53–28.23
FR4/92 PC24A	146.892833	17.864167	225	Upper slope	T1	100.5–126.5	70.0	C	92/24a_24	UBA-10573	116.8	Shell fragment within T1	22,243	73	26.29	25.89–26.69
									92/24a_23	UBA-11468	130.8	Hemipelagic mud 4 cm below T1	10,685	36	12.05	11.86–12.26
FR4/92 PC32	148.040500	17.988000	1134	Basin (nearest slope with few canyons)	T1	35.5–40	77.9	C	92/32_33	UBA-10567	40.5	Hemipelagic mud below T1	18,984	51	22.22	21.99–22.45
					T2	154–158	N.D.	I	N.A.	N.A.	N.A.	N.A.	N.D.	N.D.	N.D.	N.D.
					T3	165–169	N.D.	C?	N.A.	N.A.	N.A.	N.A.	N.D.	N.D.	N.D.	N.D.
					T4	263–264.5	N.D.	C?	N.A.	N.A.	N.A.	N.A.	N.D.	N.D.	N.D.	N.D.
					T5	298–304	77.5	C	92/32_35	UBA-10568	305	Hemipelagic mud below T5	49,240	763	53.13	51.16–55.10
					T6	351–354	29.9	S	92/32_37	UBA-10569	357	Hemipelagic mud 3 cm below T1	>58,151	1900	>58.15	

[a] Data from cores FR5/90 PC19-20-21 from Webster et al. (2012).
[b] C = carbonate-dominated turbidite; S = siliciclastic-dominated turbidite; M = mixed carbonate-siliciclastic turbidite; I = indeterminate turbidite; ? = turbidite type based on the interpretation of the sedimentary context.
[c] OZJ# & OZL# AMS-C14 analyses were measured at Australian Nuclear Science and Technology Organisation (ANSTO); UBA-# AMS-C14 analyses were measured at the 14CHRONO Centre, Queens University Belfast.
[d] SGF = sediment gravity flow.
[e] N.A. = not applicable.
[f] N.D. = not determined.

Table 2
Location of cores in other studies.

Core number	Longitude (°E)	Latitude (°S)	Depth (m)	Depositional context[a]
Page et al. (2003) study cores				
FR5/90 PC27A	145.946667	15.290000	2163	Basin floor (lower slope). Close to landslide scar
FR4/92 PC11	147.347500	17.571167	1320	Basin floor
FR4/92 PC12	147.142167	17.267167	1443	Basin floor
FR4/92 PC13	146.919333	16.951333	1507	Basin floor
FR4/92 PC14	146.732333	16.722833	1574	Basin floor (middle slope)
GC43	147.476666	18.132833	901	Base of the slope. Close to lower slope landslides
ODP Leg 133 Sites				
819	146.325000	16.624000	565	Middle slope
820	146.304000	16.637000	279	Upper slope
821	146.290000	16.647000	213	Upper slope

[a] Interpretation based on high-resolution multibeam bathymetry used in this study. Text in brackets shows original interpretation.

2000; Page et al., 2003), but not necessarily funneled through the deep canyons.

Despite the overall differences in the turbidite deposition pattern, the Noggin Passage and Ribbon Reef turbidite depositional systems share some characteristics. Siliciclastic turbidite deposition in the Noggin Passage region is restricted to the lowest sea level (22–16 ka ago; Fig. 3B) and it was supplied by one of the few canyons in the region that breaches the shelf-edge (Fig. 1C). This situation is similar to that found in the Ribbon Reef region (e.g. Canyon 6; 90/26) and confirms the importance of shelf-breaching in the transport of coarse-grained siliciclastic sediments through the canyons. The deposition of carbonate turbidites in the Noggin Passage region during the MIS2 sea-level lowstand is consistent with the Ribbon Reef region (see Webster et al., 2012). Similarly, carbonate turbidite deposition during the sea-level highstand period supports predictions by the highstand shedding model. During the interglacial sea-level highstand, the carbonate factory on the shelf was fully turned on.

The Palm Passage region records scarce turbidite deposition compared with the Ribbon Reef and Noggin Passage regions (Figs. 2C and 3C), and comprises carbonate turbidites and an old (>58 ka) siliciclastic event. Although the source and sediment pathways are not as well defined, the model of turbidite deposition in the Palm Passage region can also be understood in terms of the margin physiography. The general absence of turbidites in the Palm Passage region relates to the fewer canyons excavating the slope, which might act as preferential pathways for sediment transport to the basin. The solitary turbidite in core 92/16 (Figs. 1 and 2C) is likely related to one of the small, lower slope canyons excavated into a large scarp at the base of the slope (Fig. 1D). The carbonate production and hemipelagic shedding during the sea-level fluctuations across the shelf-break was similar to the Noggin Passage region, although in the Palm Passage region, the extent of the shelf flooded was wider (Fig. 3D). The presence of ~26 ka old bioclastic material (including coral fragments) in a turbidite emplaced ~12 ka ago on the upper slope (92/24A; Fig. 2C) suggests a source when the sea level was at ~75–80 m below the present sea level. Similar to the Noggin Passage region, the Palm Passage region has extensive drowned shelf-edge reefs that could supply these carbonate sediments. The abundant landslides which characterize the Palm Passage region could also be local, but important, sediment sources to the basin as slide material can evolve downslope into sediment gravity flows (Hampton, 1972). Due to the overall lack of connection with the shelf in the Palm Passage region, we speculate that some of these sediment flows may be associated with the older turbidite events. Both within and between the three study regions, there is no coherent pattern that suggests any strong relationship between turbidite thickness and sea-level variation.

Table 3
Relative abundance of turbidite types in the north-eastern Australia margin.

	Turbidite relative abundance (%)[a]			
	C[b]	M	S	I
Full region	61.7	12.3	14.8	11.1
RR	37.8	27.0	21.6	13.5
NP	83.3	0	8.3	8.3
PP	75.0	0	12.5	12.5

[a] Based on 81 turbidites.
[b] C = carbonate-dominated turbidite; S = siliciclastic-dominated turbidite; M = mixed carbonate-siliciclastic turbidite; I = indeterminate turbidite; RR = Ribbon Reef region; NP = Noggin Passage region; PP = Palm Passage region.

Well-constrained examples of turbidite deposition at millennial scale in other large mixed carbonate-siliciclastic systems are scarce. The most comparable example to the north-eastern Australia margin is the Gulf of Papua (Francis et al., 2008). In this region, high-resolution turbidite chronology goes back through the last 22 ky (Jorry et al., 2008, 2010) and therefore it is difficult to fully compare this record to our model. In the Gulf of Papua, there is a change in the type of turbidites, from siliciclastic turbidites prior to 11 ky to a calciturbidite at about 11 ky related to the first reflooding of the carbonate bank tops, and then during the Holocene, the record corresponds to fine-grained platform-derived neritic sediments (Jorry et al., 2008). Such turbidite depositional timing is not entirely in agreement with our observations of the north-eastern Australia margin. In the Gulf of Papua, carbonate turbidites are sourced from carbonate banks and atolls, which are disconnected from the main land-attached platform and therefore siliciclastic and carbonate turbidites do not share the same shelf-to-slope sediment pathways (i.e. submarine canyons) as occurs on the north-eastern Australian margin.

The turbidite deposition model presented here is also consistent with the detailed geomorphic framework of canyon systems and shelf-edge morphology in the north-eastern Australia margin (Abbey et al., 2011; Puga-Bernabéu et al., 2011, 2013). Future work must focus on testing this model in other regions worldwide and over several glacial–interglacial cycles, either along the north-eastern Australia margin or within the ancient sedimentary record.

6. Conclusions

Turbidite deposition along the north-eastern Australia margin over the last 60 ky shows a variety of patterns that result from the interaction of sea-level fluctuations across the shelf-break, and importantly, are influenced by the variations in shelf-edge physiography, in particular the canyon and shelf-edge morphology. As a result, turbidite deposition along the north-eastern Australia margin can either be consistent or diverge from the existing models of margin sedimentation (i.e. reciprocal, highstand shedding and coeval models) depending on the variable physiography at the margin. Our study reveals that:

1) The influx of siliciclastic and mixed carbonate-siliciclastic turbidites is mainly controlled by the presence of canyons indenting the shelf-break, which preferentially capture siliciclastic sediments stored or bypassing the shelf. This process, ultimately controlled by the position of sea level, is favored by the presence of effective shelf-edge reef barriers, which block and store the sediment behind them, and concentrating the sediment fluxes through the inter-reef passages.

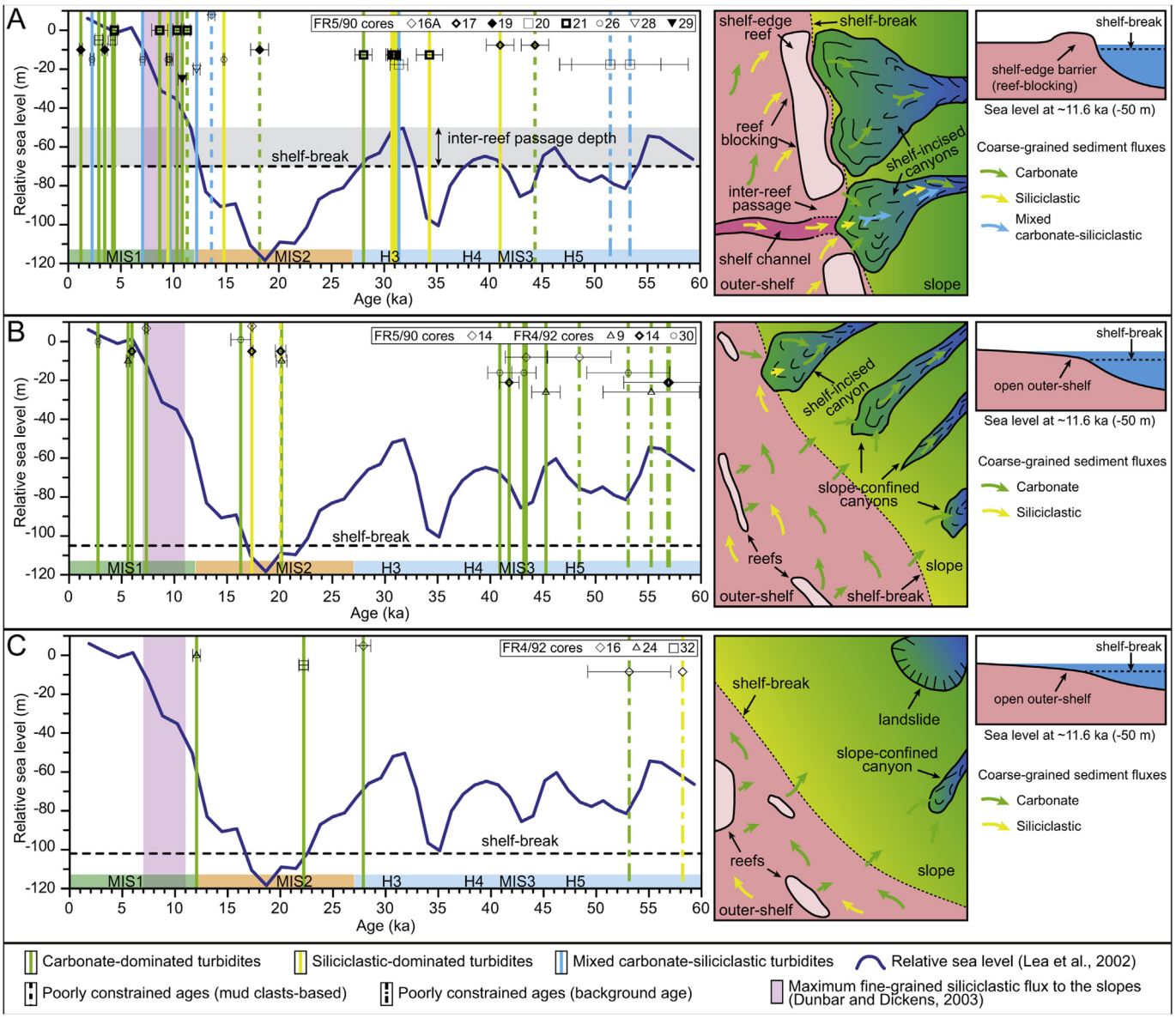

Figure 3. Relationship between turbidite composition, depositional timing and Late Pleistocene sea-level change (Lea et al., 2002) in (A) Ribbon Reef, (B) Noggin Passage, and (C) Palm Passage regions. Turbidite ages are plotted against relative sea-level record. Turbidite chronology corresponds to the maximum age of turbidite emplacement (see methods section for discussion of potential biases). Error bars correspond to the 2σ age range from the calibrated ages BP (ka). Marine isotope stages (MIS 3-1), Heinrich events (H5-3), and the period of maximum flux of fine-grained, hemipelagic siliciclastic sediments to the slope and basin of the north-eastern Australia margin (Dunbar and Dickens, 2003) are also shown. Plan view maps illustrate the main physiographic characteristics and interpreted coarse-grained sediment pathways. Cross sections show the gereralized differences in shelf flooding across the margin during the late transgression.

Table 4
Summary of the dominant turbidites types along the north-eastern Australia margin within the context of eustatic sea-level variability, shelf-edge moprphology and canyons type.

Region	Outer-shelf morphology	Dominant canyon type and slope morphology	Dominant turbidite type during different sea level positions		
			Lowstand sea level	Transgressive sea level or equivalent sea-level height	Highstand sea level
Ribbon Reef	Flat, extensive shelf-edge barrier reef Shelf-break at ~70 m	Shelf-incised Narrow steep slope	Carbonate Siliciclastic	Siliciclastic Mixed carbonate-siliciclastic Carbonate	Carbonate Mixed carbonate-siliciclastic
Noggin Passage	Gently sloping, open conditions Shelf-break at ~105 m	Slope-confined, locally shelf-incised Moderate slopes	Carbonate Locally siliciclastic (related to shelf-incised canyons)	Carbonate	Carbonate
Palm Passage	Gently sloping, open conditions Shelf-break at ~102 m	Slope-confined and landslides Wide, moderate to gentle slope	Carbonate	Carbonate	Carbonate (?)

2) Carbonate turbidite deposition dominates in regions with more open (i.e. little or no reef blocking) conditions at the outer-shelf, and on slopes excavated by slope-confined canyons or where canyons are less abundant.
3) Carbonate turbidites were deposited either as a result of the reflooding of the shelf during the late transgression or when the shelf-edge configuration created a depth window for greater carbonate production during MIS 3 lowered sea-level periods.

These findings suggest that generic sequence stratigraphic models of mixed carbonate-siliciclastic depositional systems and dominated by extensive reef development should be revised to account for variations in sediment supply driven by any major changes in the margin physiography.

Acknowledgments

This research was funded by the Australian Marine National Facility, James Cook University, Nederlands Centrum voor Biodiversiteit, the University of Sydney and the Research Group RNM-190 of the Junta de Andalucía (Spain). We also thank to "Subprograma de Técnicos de Apoyo MICINN (PTA2009-1782-I)" for carbon content analyses. Constructive reviews by Morelia Urlaub and Bradley Opdyke are greatly appreciated.

References

Abbey, E., Webster, J.M., Beaman, J., 2011. Geomorphology of submerged reefs on the shelf edge of the Great Barrier Reef: the influence of oscillating Pleistocene sea-levels. Mar. Geol. 288, 61–78.
Baztan, J., Berné, S., Olivet, J.-L., Rabineau, M., Aslanian, D., Gaudin, M., Réhault, J.-P., Canals, M., 2005. Axial incision: the key to understand submarine canyon evolution (in the western Gulf of Lion). Mar. Pet. Geol. 22, 805–826.
Beaman, R.J., 2010. 3DGBR. A High-resolution Depth Model for the Great Barrier Reef and Coral Sea. Marine and Tropical Sciences Research Facility (MTSRF). Project 2.5i.1a Final Report, MTSRF, 13 pp. Plus Appendix 1 http://www.deepreef.org/bathymetry/65-3dgbr-bathy.html (accessed June 2013).
Beaubouef, R.T., Rossen, C., Zelt, F.B., Sullivan, M.D., Mohrig, D.C., Jennette, D.C., 1999. Deep-water sandstones of the Brushy canyon Formation, west Texas, Field Guide. In: American Association of Petroleum Geologists, Hedberg Field Research Conference, April 15–20, p. 48.
Bornhold, B.D., Pilkey, O.H., 1971. Bioclastic turbidite sedimentation in Columbus Basin, Bahamas. Geol. Soc. Am. Bull. 82, 1341–1354.
Covault, J.A., Romans, B.W., 2009. Growth patterns of deep-sea fans revisited: turbidite-system morphology in confined basins, examples from the California Borderland. Mar. Geology. 265, 51–66.
Crevello, P.D., Schalger, W., 1980. Carbonate debris sheets and turbidites, Exuma Sound, Bahamas. J. Sediment. Petrol. 50, 1121–1148.
Davies, P.J., McKenzie, J.A., Palmer-Julson, A., et al., 1991. In: Proceedings of the Ocean Drilling Program Initial Reports, 133. Ocean Drilling Program, College Station, TX. In: http://dx.doi.org/10.2973/odp.proc.ir.133.1991.
Droxler, A.W., Schalger, W., 1985. Glacial versus interglacial sedimentation rates and turbidite frequency in the Bahamas. Geology 13, 799–802.
Druffel, E.R.M., Griffin, S., 1993. Large variations of surface ocean radiocarbon: evidence of circulation changes in the southwestern Pacific. J. Geophys. Res. 98 (C11), 20249–20259.
Druffel, E.R.M., Griffin, S., 1999. Variability of surface ocean radiocarbon and stable isotopes in the southwestern Pacific. J. Geophys. Res. 104 (C10), 23607–23613.
Ducassou, M., Migeon, S., Mulder, T., Murat, A., Capotondi, L., Bernasconi, S.M., Mascle, J., 2009. Evolution of the Nile deep-sea turbidite system during the Late Quaternary: influence of climate change on fan sedimentation. Sedimentology 56, 2061–2090.
Dunbar, G.B., Dickens, G.R., 2003. Massive siliciclastic discharge to slopes of the Great Barrier Reef Platform during sea-level transgression: constraints from sediment cores between 15° and 16° latitude and possible explanations. Sediment. Geol. 162, 141–158.
Dunbar, G.B., Dickens, G.R., Carter, R.M., 2000. Sediment flux across the Great Barrier Reef Shelf to the Queensland Trough over the last 300 ky. Sediment. Geol. 133, 49–92.
Francis, J.M., Dunbar, G.B., Dickens, G.R., Sutherland, I.A., Droxler, A.W., 2007. Siliciclastic sediment across the North Queensland Margin (Australia). A Holocene perspective on reciprocal versus coeval deposition in tropical mixed siliciclastic-carbonate systems. J. Sediment. Res. 77, 572–586.
Francis, J.M., Daniell, J.J., Droxler, A.W., Dickens, G.R., Bentley, S.J., Peterson, L.C., Opdyke, B.N., Beaufort, L., 2008. Deep water geomorphology of the mixed siliciclastic-carbonate system, Gulf of Papua. J. Geophys. Res. 113. http://dx.doi.org/10.1029/2007JF000851 (F01S16).
Goldfinger, C., Morey, A.E., Nelson, C.H., Gutierrez-Pastor, J., Johnson, J.E., Karabanov, E., Chaytor, J., Eriksson, A., 2007. Rupture lengths and temporal history of significant earthquakes on the offshore and north coast segments of the Northern San Andreas Fault based on turbidite stratigraphy. Earth Planet. Sci. Lett. 254, 9–27.
Hampton, M., 1972. The role of subaqueous debris flow in generating turbidity currents. J. Sediment. Petrol. 42, 775–793.
Jorry, S.J., Droxler, A.W., Mallarino, G., Dickens, G.R., Bentley, S.J., Beaufort, L., Peterson, L.C., Opdyke, B.N., 2008. Bundled turbidite deposition in the central Pandora Trough (Gulf of Papua) since Last Glacial Maximum. Linking sediment nature and accumulation to sea level fluctuations at millennial timescale. J. Geophys. Res. 113, F01S19. http://dx.doi.org/10.1029/2006JF000649.
Jorry, S.J., Droxler, A.W., Francis, J.M., 2010. Deepwater carbonate deposition in response to re-flooding of carbonate bank and atoll-tops at glacial terminations. Quat. Sci. Rev. 29, 2010–2026.
Lea, D.W., Martin, P.A., Pak, D.K., Spero, H.J., 2002. Reconstruction a 350 ky history of sea-level using planktonic Mg/Ca and oxygen isotope records from a Cocos Ridge core. Quat. Sci. Rev. 283, 283–293.
Owen, M., Day, S., Maslin, M., 2007. Late Pleistocene submarine mass movements: occurrence and causes. Quat. Sci. Rev. 26, 958–978.
Page, M.C., Dickens, G.R., Dunbar, G.B., 2003. Tropical view of Quaternary sequence stratigraphy. Siliciclastic accumulation on slopes east of the Great Barrier Reef since the Last Glacial Maximum. Geology 31, 1013–1016.
Posamentier, H.W., Vail, P.R., 1988. Eustatic control on clastic deposition II – sequence and system tracts models. In: Wilgus, C.K., Hastings, B.S., Posamentier, H., Van Wagoner, J., Ross, C.A., Kendall, C.G.St.C. (Eds.), Sea Level Changes: an Integrated Approach, SEPM Special Publication 42, pp. 125–154.
Puga-Bernabéu, Á., Webster, J.M., Beaman, R.J., Guilbaud, V., 2011. Morphology and controls on the evolution of a mixed carbonate-siliciclastic submarine canyon system, Great Barrier Reef margin, north-eastern Australia. Mar. Geol. 289, 100–116.
Puga-Bernabéu, Á., Webster, J.M., Beaman, R.J., Guilbaud, V., 2013. Variation in canyon morphology on the Great Barrier Reef margin, north-eastern Australia: the influence of slope and barrier reefs. Geomorphology 191, 35–50.
Reimer, P.J., Baillie, M.G.L., Bard, E., Bayliss, A., Beck, J.W., Blackwell, P.G., Bronk Ramsey, C., Buck, C.E., Burr, G.S., Edwards, R.L., Friedrich, M., Grootes, P.M., Guilderson, T.P., Hajdas, I., Heaton, T.J., Hogg, A.G., Hughen, K.A., Kaiser, K.F., Kromer, B., McCormac, F.G., S.W Manning, Reimer, R.W., Richards, D.A., Southon, J.R., Talamo, S., Turney, C.S.M., van der Plicht, J., Weyhenmeyer, C.E., 2009. INTCAL09 and MARINE09 radiocarbon age calibration curves, 0–50,000 years Cal BP. Radiocarbon 51, 1111–1150.
Tilbrook, B., Matear, R., 2008. Carbon Chemistry of the Great Barrier Reef: RV Southern Surveyor – Voyage Summary. Marine National Facility, p. 17. In: http://www.cmar.csiro.au/datacentre/process/data_files/cruise_docs/SS200809sum.pdf (accessed November 2013).
Ulm, S., 2002. Marine and estuarine reservoir effects in Central Queensland, Australia: determination of ΔR values. Geoarchaeol. Int. J. 17, 319–348.
Webster, J.M., Davies, P.J., Beaman, R.J., Williams, S., Byrne, M., 2008. Evolution of Drowned Shelf Edge Reefs in the GBR; Implications for Understanding Abrupt Climate Change, Coral Reef Response and Modern Deep Water Benthic Habitats: RV Southern Surveyor – Voyage Summary. Marine National Facility, p. 18. http://www.marine.csiro.au/nationalfacility/voyagedocs/2007/summarySS07-2007.pdf (accessed November 2013).
Webster, J.M., Beaman, R.J., Puga-Bernabéu, Á., Ludman, D., Renema, W., Wust, R.A.J., George, N.P.J., Reimer, P.J., Jacobsen, G.E., 2012. Source, timing, and controls on turbidite sedimentation in the submarine canyons off the northern Great Barrier Reef, Australia. Palaeogeogr. Palaeoclimatol. Palaeoecol. 331–332, 75–89.
Webster, J.M., Yokoyama, Y., Cotterill, C., the Expedition 325 Scientists, 2011. In: Proceedings of the Integrated Ocean Drilling Program, vol. 325. Integrated Ocean Drilling Program Management International, Inc, Tokyo.
Weninger, B., Jöris, O., Danzeglocke, U., 2007. CalPal-2007. Cologne Radiocarbon Calibration & Palaeoclimate Research Package.
Wilson, J.L., 1967. Cyclic and reciprocal sedimentation in Virgilian Strata of southern New Mexico. Geol. Soc. Am. Bull. 78, 805–818.